Check for updates

BIOPHYSICS

Ligand-tuned extracellular domain dynamics are correlated with signaling states in an adhesion GPCR

Kristina Cechova[1], Sumit J. Bandekar[2,3,4,5], Szymon P. Kordon[2,3,4,5], Max Foroutan[1], Katherine Leon[2,3,4,5], Gracie Siffer[1], Michael R. Schamber[1], Maria Luiso[1], Demet Araç[2,3,4,5]*, Reza Vafabakhsh[1]*

Copyright © 2026 The Authors, some rights reserved; exclusive licensee American Association for the Advancement of Science. No claim to original U.S. Government Works. Distributed under a Creative Commons Attribution NonCommercial License 4.0 (CC BY-NC).

Adhesion G protein–coupled receptors (aGPCRs) transduce signals via engagement of their large extracellular regions (ECRs) with adhesion partners. ADGRG6 (GPR126) is an aGPCR vital for the development of multiple organs and myelination. ECR conformational dynamics of ADGRG6 has been shown to modulate aGPCR signaling and in vivo function. Yet, how adhesion partners regulate ECR conformational dynamics is poorly understood. Here, we studied activation of ADGRG6 using single-molecule FRET (smFRET) and intracellular signaling assays. We reveal that the ADGRG6 ECR dynamically transitions between three conformational states. Covalently locking the ECR in the closed conformation traps the receptor in a low-activity state. Agonist binding physically restricts the ECR to only access states associated with higher activity. This detailed mechanistic insight into ADGRG6 allosteric regulation by ECR dynamics offers avenues for targeted therapeutic development.

INTRODUCTION

The extracellular domains of many cell surface receptors serve as specialized gateways, initiating signal transduction via molecular recognition and ligand binding. These domains often adopt multiple conformations that are associated with distinct downstream signaling outcomes. These conformational dynamics enable generation of diverse cellular responses and offer potential for therapeutic intervention through targeted modulation of receptor states. For example, the conformational states of integrins and epidermal growth factor receptors have been targeted to modulate cellular responses and treat diseases (*1*, *2*). For many other receptors, however, the full conformational repertoire of their extracellular domains and how specific structural states correlate with specific signaling outcome remains unclear.

The adhesion G protein–coupled receptors (aGPCRs) represent a relatively understudied GPCR family that has key roles in neurobiological, developmental, and immunological functions and are involved in numerous human diseases including brain malformations, attention deficit hyperactivity disorder, cancers, and male infertility (*3*–*5*). aGPCRs are characterized by a large extracellular region (ECR) that is typically modular, with multiple tandem domains, many with adhesion properties (Fig. 1A). Common to almost all aGPCRs is the GPCR autoproteolysis-inducing (GAIN) domain, located proximally to the seven-transmembrane domain (7TMD) (*3*, *6*, *7*). In most aGPCRs, the GAIN domain mediates autoproteolytic cleavage generating an N-terminal fragment encompassing most of the ECR and a C-terminal fragment containing the 7TMD and intracellular regions. These fragments remain tightly associated after integration of the receptor in the plasma membrane (*6*). The tethered agonist-dependent mechanism of activation of aGPCRs proposes that ligand binding and mechanical stimuli result in dissociation of the two fragments, exposing a short peptide called Stachel peptide that functions as a tethered agonist to activate the receptor via orthosteric site engagement (Fig. 1A) (*8*, *9*). Recent structures of the truncated transmembrane domains of different aGPCRs have revealed the structural basis of tethered agonist activation mode for aGPCRs (*10*–*13*). Yet, animal models in which autoproteolysis was blocked by point mutations still exhibited signaling in vivo, pointing to versatile nature of signaling in aGPCRs (*14*–*16*). In such an ECR-dependent mechanism of activation, the ECR senses ligand binding and mechanical stimuli via direct conformational coupling between the ECR and the 7TMD while they are still associated (Fig. 1A) (*15*, *17*–*23*). In support of this model, perturbations to the ECR and conformational changes within the ECR have been shown to correlate with changes in downstream signaling in different aGPCRs (*22*–*28*). Previous structural work also showed that the ECRs of aGPCRs, sample varying defined conformations that range from "compact/closed" to "extended/open-like" conformations (*25*, *29*). Last, the cryo–electron microscopy (cryo-EM) structure and single-molecule dynamic studies of a holoadhesion GPCR revealed that the ECR has restricted defined conformations with respect to the 7TMD and communicates with the transmembrane domain to modulate receptor signaling (*24*). However, the molecular basis of the conformational changes that occur within the ECR of aGPCRs upon ligand binding is generally unclear.

aGPCR G6 (ADGRG6 or GPR126) is a large aGPCR with an ECR of 850 amino acids. ADGRG6 plays critical roles in Schwann cell differentiation and myelination, cardiovascular system development, and osteogenesis (*30*–*32*). ADGRG6 has also been implicated in cancer progression, congenital scoliosis, chronic obstructive pulmonary disease, and peripheral neuropathies (*31*, *33*–*36*). Multiple ligands interact with the ECR of ADGRG6, and these interactions are shown to be important for cell adhesion and differentiation. Specifically, type IV collagen (Coll IV) and laminin-211, major components of the basal lamina, were shown to activate ADGRG6 and increase the cyclic adenosine 3′,5′-monophosphate (cAMP) levels (*21*, *37*, *38*). Last, the cellular prion protein (PrP^C) was identified as an agonist of ADGRG6 and was shown to elevate cAMP (*39*). The precise molecular mechanisms by which ligand-ECR engagement allosterically activates ADGRG6 remain unresolved.

[1]Department of Molecular Biosciences, Northwestern University, Evanston, IL, USA. [2]Department of Biochemistry and Molecular Biology, The University of Chicago, Chicago, IL, USA. [3]Neuroscience Institute, The University of Chicago, Chicago, IL, USA. [4]Institute for Biophysical Dynamics, University of Chicago, Chicago, IL, USA. [5]Center for Mechanical Excitability, The University of Chicago, Chicago, IL, USA.
*Corresponding author. Email: arac@uchicago.edu (D.A.); reza.vafabakhsh@northwestern.edu (R.V.)

Downloaded from https://www.science.org on October 07, 2026

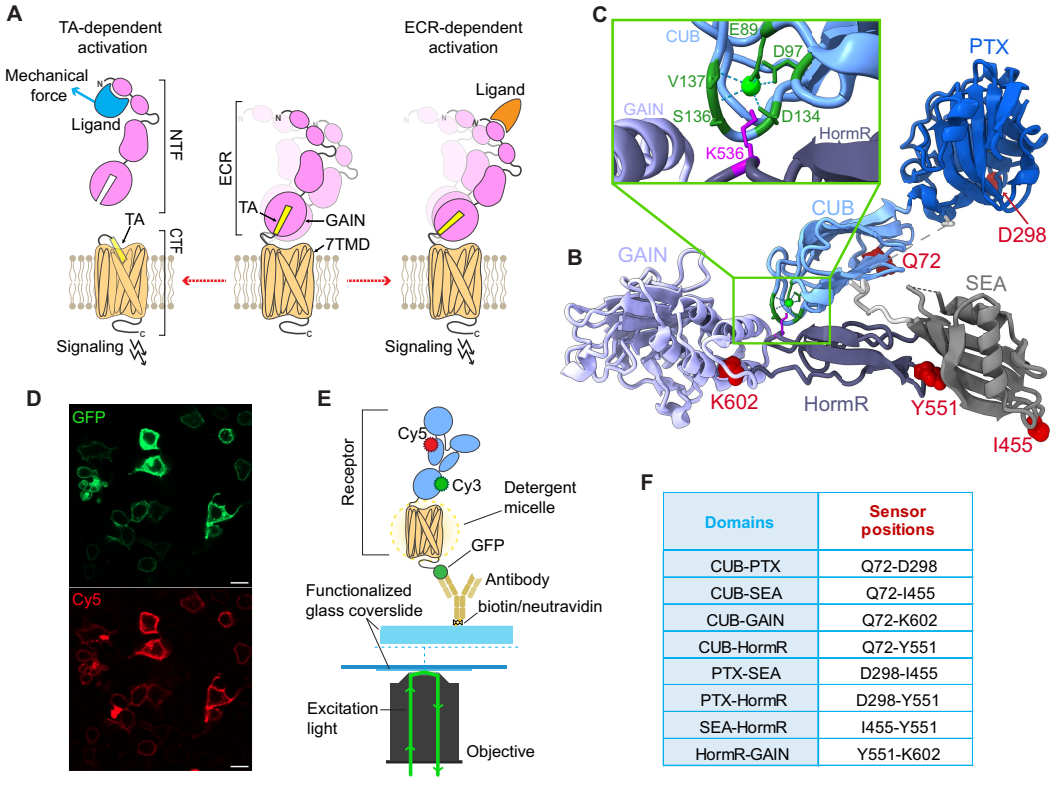

Domains	Sensor positions
CUB-PTX	Q72-D298
CUB-SEA	Q72-I455
CUB-GAIN	Q72-K602
CUB-HormR	Q72-Y551
PTX-SEA	D298-I455
PTX-HormR	D298-Y551
SEA-HormR	I455-Y551
HormR-GAIN	Y551-K602

Fig. 1. Experimental system to probe the activation of ADGRG6. (**A**) Proposed activation mechanisms of aGPCRs consisting of tethered agonist (TA)–dependent and ECR-dependent modes. (**B**) Structure of zfADGRG6 extracellular domains [Protein Data Bank (PDB): 6v55] in closed conformation, amino acids in red denote the labeling positions in each domain. (**C**) Close-up view of the calcium ion (green circle) coordinated by five amino acid residues of CUB domain and interaction of CUB and HormR domains mediated by lysine-536 on HormR (purple). (**D**) Confocal microscopy images of cells expressing ADGRG6-GFP with one unnatural amino acid at position 551 labeled with Cy5. Scale bars, 10 μm. (**E**) Schematic of receptor surface immobilization for smFRET experiments. (**F**) Table of amino acid pair positions used in smFRET experiments. NTF, N-terminal fragment; CTF, C-terminal fragment.

The ECR of ADGRG6 comprises five domains: a CUB (complement subcomponents C1r/C1s, Uegf, and Bmp1) domain, a PTX (pentraxin) domain, a SEA (sperm protein, enterokinase, and agrin) domain, a hormone binding (HormR) domain, and the GAIN domain (*25*) (Fig. 1B). The crystal structure of zebrafish ADGRG6 ECR shows the overall arrangement of these five domains in a "closed ECR conformation" with a calcium ion positioned at the CUB-HormR-GAIN interface, suggesting a role for calcium in maintaining the closed conformation (Fig. 1, B and C) (*25*). A transgenic zebrafish carrying point mutations at the calcium-binding site perturb the closed conformation and exhibit an "open-like ECR conformation" (*25*). This zebrafish mutant shows severe phenotypes in peripheral nervous system myelination and ear development, which both depend on downstream receptor signaling (*25*). These results suggested a key role for an "ECR conformational switch" in vivo and indicate that ECR conformational regulated receptor signaling and function (*25*). Another ADGRG6 isoform (referred to as the +ss isoform), which incorporates a 23–amino acid insertion in a linker within the ECR, displayed an open-like conformation with increased basal signaling (*25*). This demonstrates that the ADGRG6 ECR can adopt alternative conformations, and these structural states regulate receptor signaling. In ADGRG6, alternative splicing within the ECR modulates the distribution of these conformational populations (*25*). As shown in ADGRG6 and multiple other aGPCRs, distinct ECR conformations can correlate with different levels of receptor activity (*22*, *24*, *25*).

Here, we used single-molecule Förster resonance energy transfer (smFRET) imaging (*40*), signaling assays, mutagenesis, and cross-linking to map the conformational landscape of zebrafish ADGRG6 extracellular domains and uncover the functional-conformational relationships of this adhesion receptor. We show that the ECR of zfADGRG6 is intrinsically dynamic, sampling distinct conformational states linked to different signaling levels. We demonstrate that the equilibrium between these states is controlled by ligand binding, thereby modulating receptor activity. Our results suggest a mechanism for ADGRG6 activation by agonists where, rather than inducing local conformational changes, ligands physically restrict access to certain receptor conformational states with lower activity, thereby promoting signaling. These findings could provide a foundation for developing synthetic ADGRG6 agonists and antagonists with therapeutic potential and could likely be expandable to other aGPCRs.

RESULTS

Mapping the interdomain conformational arrangement of ADGRG6 ECR

To characterize the intrinsic conformational fluctuations within the ADGRG6 ECR and how these changes modulate receptor function,

Downloaded from https://www.science.org on October 07, 2026

we first mapped the conformational landscape of zebrafish ADGRG6 using smFRET (*40*). Using the available crystal structure of zfADGRG6 isoform that excludes a 23–amino acid segment between the PTX and SEA domains (−ss isoform) (*25*, *41*), we generated FRET sensors with donor and acceptor pairs positioned on different domains within the ECR (Fig. 1B) to obtain an interdomain conformational map of the ECR. To achieve site-specific labeling, we used the incorporation of the unnatural amino acid trans-cyclooct-2-en-L-lysine on specific positions (Fig. 1B), followed by copper-free click chemistry reaction for fluorescent labeling with tetrazine-conjugated cyanine3 (Cy3) (donor) and cyanine5 (Cy5) (acceptor) dyes (*24*, *42*). Last, a C-terminal mEGFP was used for screening for expression validation (Fig. 1D). Fluorescent labeling was performed in live cells to selectively label membrane-localized receptors (Fig. 1D). The full-length receptors were isolated, and their purity was confirmed by polyacrylamide gel analysis (fig. S1A). To ensure that fluorophore incorporation did not compromise receptor function, we verified that the engineered receptor sensors elevated cAMP concentration in cells at levels comparable to wild-type (WT) receptor (fig. S1B). For smFRET experiments, receptors were immobilized on a biotinylated polyethylene glycol (PEG)–passivated surface functionalized with neutravidin and a biotinylated anti-GFP antibody (Fig. 1E) (*24*, *43*).

We generated eight FRET sensors for in-depth analysis to probe the ECR dynamics of ADGRG6 (Fig. 1F). Since calcium was observed at the interface between the CUB and GAIN and HormR domains and point mutations D134A/F135A at the calcium binding site were shown to disrupt calcium coordination leading to open-like conformational states (Fig. 1, B and C), it was proposed to have a stabilizing role for maintaining the closed conformation (*25*). This idea was further supported by the notable developmental defects in zebrafish harboring the same mutations that disrupt the closed conformation (*25*). smFRET traces in the presence of 5 mM calcium revealed two distinct behaviors for the sensors: Some sensors showed stable FRET values with a narrow single-peak FRET distribution, while others showed dynamic anticorrelated transitions between multiple states, producing broad histogram distributions (Fig. 2, A and B, and fig. S2). Specifically, sensors monitoring movement between the SEA, HormR, and GAIN domains show limited dynamics, as do sensors monitoring movement between the CUB and PTX domains. (Fig. 2B). The excess kurtosis analysis of FRET histograms also showed that the sensors split into two groups with low structural flexibility regions and regions with more extensive structural flexibility (Fig. 2C). Last, quantification of receptor dynamics using the cross-correlation of donor and acceptor signals further showed notable differences in dynamics between the two sets of sensors (Fig. 2D). Considering the structure and overall domain arrangements (Fig. 1B), this suggests that ECR moves as two conformational units of the CUB-PTX arm and SEA-HormR-GAIN arm, with limited intra-unit flexibility (Fig. 2E), in agreement with our previous electron microscopy work (*25*) and recent molecular dynamic simulation (*26*). Since the fluorescent probes are on the ECR and the proteins are immobilized via their C-terminal tail, all the data are from intact receptors with ECR still attached.

To further characterize the conformational changes in our assay (Fig. 2A) and to test whether the movement reflects discrete, well-defined states or rather represents continuous conformation changes within a range, we focused on the CUB to GAIN domain sensor. This sensor should be able to detect conformational changes suggested by negative stain EM and small-angle x-ray scattering and molecular dynamic studies of ADGRG6 ECR isoforms, distinguishing between a compact "closed" state, with CUB, GAIN, and HormR domains right next to each other similar to the crystal structure (Fig. 1B) (*25*, *26*), or an extended "open" state in which these domains are separated. Visual inspection and analysis of individual smFRET traces using hidden Markov modeling (HMM) identified three conformational states between the CUB and GAIN domains at low (~0.28), mid (~0.44), and high FRET (~0.59) (Fig. 2, F and G, and fig. S3A). In this sensor, many molecules visited more than one state before photobleaching (fig. S3B), and the percentage of static traces were equal between the three states (fig. S3C). Considering the available structure, the FRET state at 0.59 likely represents the reported crystal structure in the closed form (*25*). Even at 5 mM Ca^{2+}, while the receptors predominantly occupied the mid and high FRET states with 38 and 45% occupancy, respectively (Fig. 2G), the low FRET state had about 17% occupancy. This result suggests that the ECR can undergo large-scale conformational changes and occasionally visit the open state. We observed similar three state dynamics for the PTX and SEA domain sensor (fig. S3, D and E). As a comparison, single molecules of the sensor monitoring motion between the CUB and PTX domains that showed a very narrow FRET distribution (Fig. 2B) exhibited mostly a single FRET state during the observation window (fig. S3, F and G) at FRET 0.88 (fig. S3H). Last, smFRET experiments with the CUB-GAIN sensor in 1 or 5 mM Ca^{2+} showed similar FRET histogram (fig. S3I).

To explore the stabilizing role of calcium in our assay, we performed experiments in the presence of 2 mM EDTA to remove the calcium from our experimental system. Under this calcium-depleted condition, the smFRET histogram for the sensor monitoring CUB-GAIN domain dynamics showed the same three FRET states as observed in the presence of calcium but with a significant change in the occupancy of the states (Fig. 3, A and B). Specifically, the occupancy of the low FRET state at 0.28, likely the open state, increased significantly from 17 to 74%, while the occupancy of both the mid and the high FRET states decreased by about 30 and 27% each (Fig. 3, B and C). This result is consistent with the model that calcium contributes to the stabilization of the closed conformation observed in the structure. We did not observe notable changes in smFRET histograms for the domains within the rigid conformational units (fig. S4, A to C), and results from other FRET sensors to probe conformation between the two dynamic units showed a significant increase in the occupancy of the low FRET state upon removal of Ca^{2+} (figs. S4, D to F, and S5). For example, the CUB-HormR sensor showed about 43% increase in the occupancy of low FRET state upon Ca^{2+} removal (fig. S5). Last, experiments on ADGRG6 receptor with D134A/F135A double mutations that disrupt Ca^{2+} binding showed that the ECR of this receptor is mostly at an open conformation (fig. S5, E and F). These results are consistent with the role of calcium in stabilizing the closed conformation.

Locking the ECR in the closed conformation traps the receptor in a low-activity state

Previous studies showed that different ECR conformations of ADGRG6 isoforms correspond to different signaling levels of the receptor (*25*). To test the functional significance of the conformational dynamics and whether the observed conformational states of the ADGRG6 ECR have distinct functional outcomes, we used the ADGRG6+ss isoform, previously shown to exhibit elevated basal cAMP signaling (*25*). This isoform has a 23–amino acid insertion

Downloaded from https://www.science.org on October 07, 2026

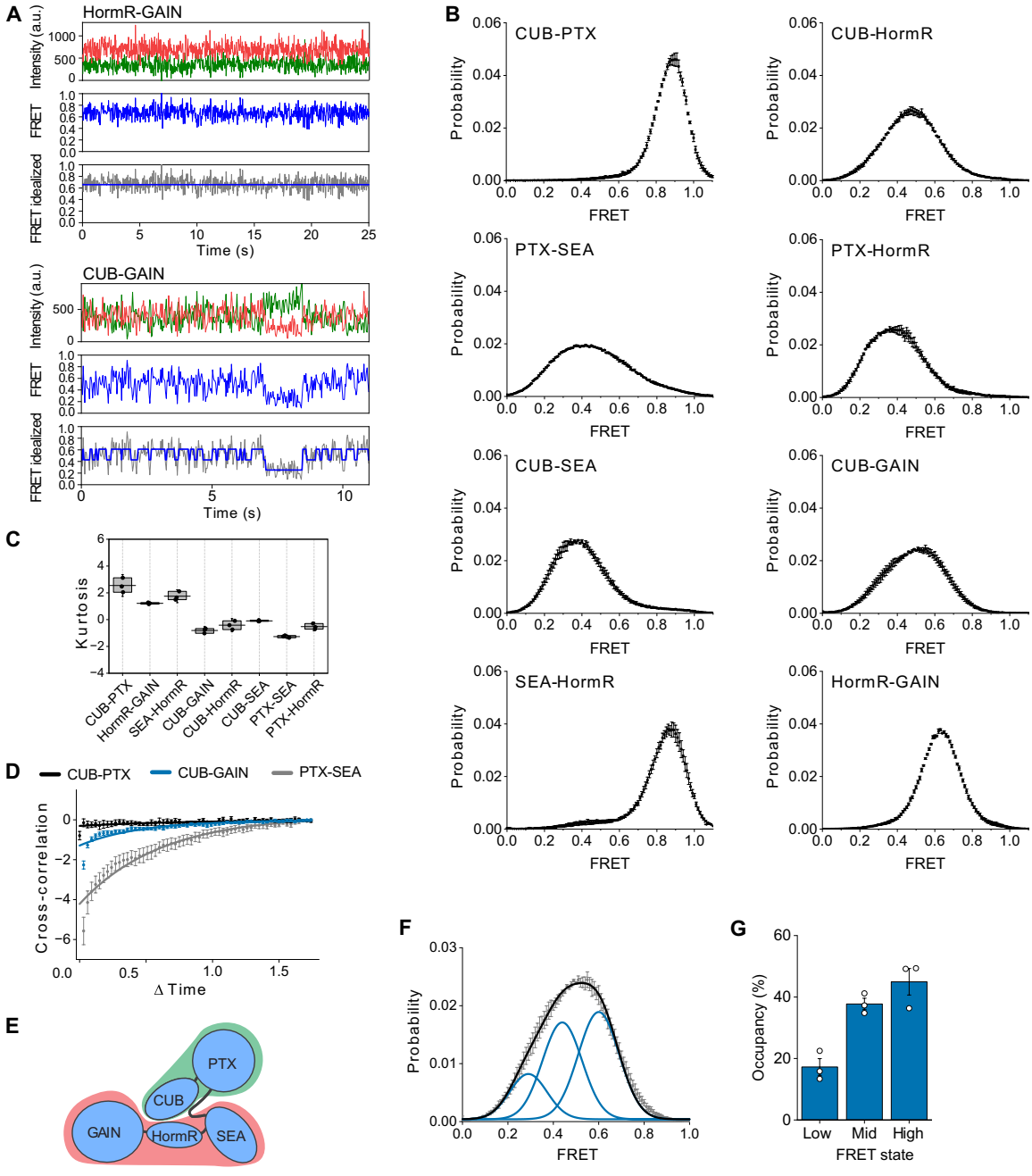

Fig. 2. The ECR of ADGRG6 undergoes complex movement. (**A**) Representative smFRET traces from sensors on HormR-GAIN and CUB-GAIN domains. a.u., arbitrary units. (**B**) smFRET population histogram in the presence of 5 mM Ca^{2+} from eight different sensor pairs on ADGRG6-ECR domains. (**C**) Box chart representing kurtosis values calculated from smFRET histograms. Boxes represent the interquartile range (25 to 75%), and the horizontal line and whiskers denote the median and the SD, $n = 3$ biological replicates. (**D**) Cross-correlation plots of selected sensor pairs representing the different dynamic behavior. Solid line represents a fit to a single exponential decay function. (**E**) Cartoon representation of ADGRG6 ECR domains highlighting two conformational unites (green and red). (**F**) smFRET population histogram from sensor pair at CUB and GAIN domain in the presence of 5 mM Ca^{2+}. Histograms were fitted with three single Gaussian distributions (blue) centered at 0.28, 0.44, and 0.59, with the cumulative fit is overlaid (black). (**G**) Bar graph representing relative occupancy of three fitted states as area under individual FRET peaks. [(B), (D), (F), and (G)] Data represent mean ± SEM of $n = 3$ independent biological replicates.

within the linker connecting the PTX and SEA domains (Fig. 3D) and is located between the two dynamic conformational units identified in our smFRET analysis and recent molecular dynamic simulations (Fig. 2E) (*26*). Notably, prior analysis of negative stain EM images and small-angle x-ray scattering experiments showed that ADGRG6+ss adopts an overall more open conformation compared to the isoform with a shorter linker (*25*). In smFRET experiments using the CUB-HormR FRET sensor in the +ss isoform and in 5 mM Ca^{2+}, the peak of FRET histogram distribution shifted to the very low FRET of ~0.13 (Fig. 3E). This low FRET population suggests a predominantly open ECR conformation for the ADGRG6+ss ECR, specifically where the CUB domain is displaced from its

Downloaded from https://www.science.org on October 07, 2026

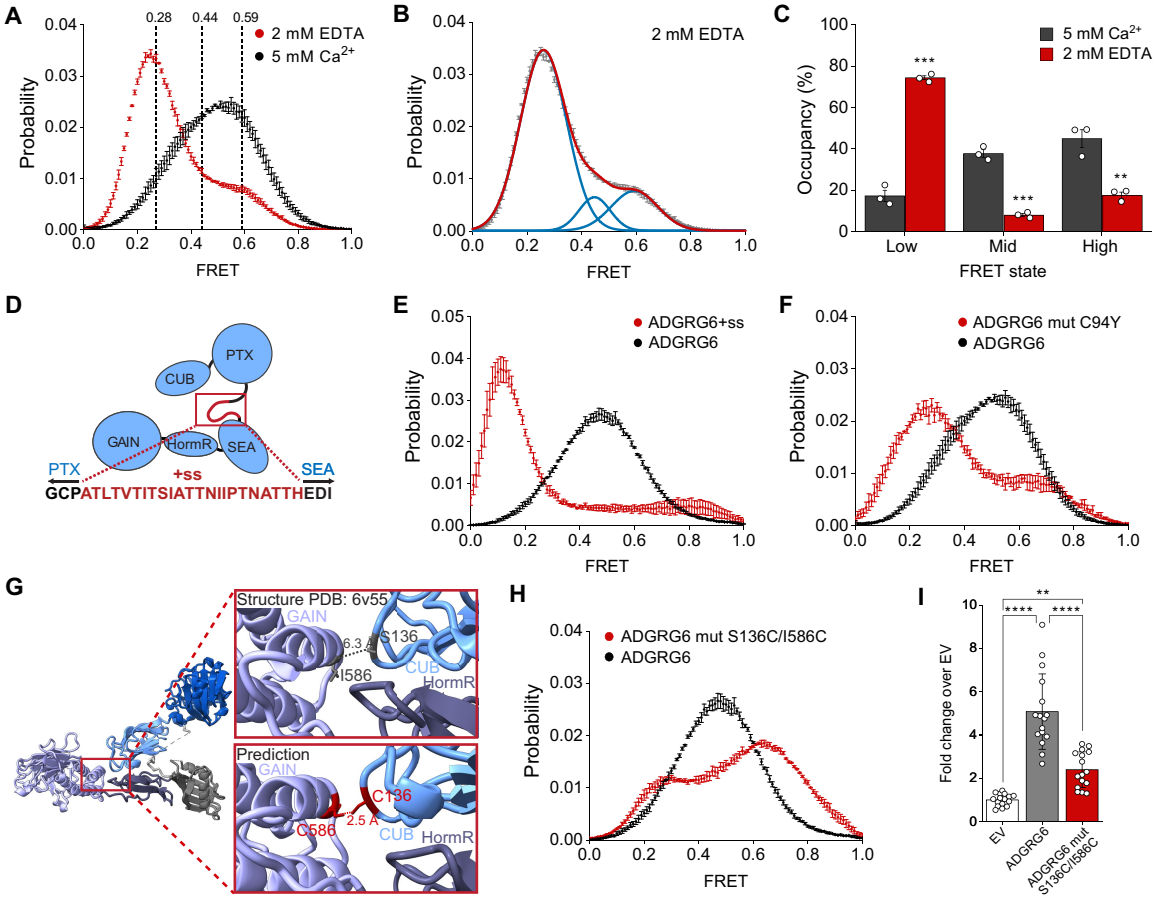

Fig. 3. Calcium modulates ECR dynamics. (**A**) Population histogram of smFRET data from sensors at CUB and GAIN domain in the presence of 5 mM Ca^{2+} or 2 mM EDTA. Vertical dashed lines indicate three FRET states. (**B**) Histogram was fitted with three single Gaussian distributions (blue) centered at 0.28, 0.44, and 0.59, and the cumulative fit is overlaid in red. (**C**) Bar graph represents relative occupancy of the three conformations. Statistical significance was determined by two-sample *t* test (***P* < 0.01 and ****P* < 0.001). (**D**) Schematic of ADGRG6 +ss isoform with 23–amino acid insertion between PTX and SEA domains. (**E**) smFRET population histogram of CUB-HormR domain sensors of two receptor variants (+ss and −ss) in 5 mM Ca^{2+} conditions. (**F**) smFRET population histogram of CUB-GAIN domain sensors for C94Y mutant and WT ADGRG6 receptors in 5 mM Ca^{2+} conditions. (**G**) Structure of zfADGRG6 ECR (PDB: 6v55) and the residues S136 and I586 from crystal structure (top) and AlphaFold2 prediction of cysteine bond formation between mutated residues C136 and C586 (bottom). (**H**) smFRET population histogram of S136C/I586C mutant compared to WT receptors in 5 mM Ca^{2+} conditions. (**I**) Signaling activity of ADGRG6 and the ADGRG6 S136C/I586C mutant measured by cAMP assay. Data are presented as fold change relative to empty vector (EV), normalized to receptor expression, and are presented as mean ± SD from three independent experiments (*n* = 16). Statistical significance was determined by one-way analysis of variance (ANOVA) followed by Tukey's multiple comparisons test. ***P* < 0.01 and *****P* < 0.0001. [(A) to (C), (E), (F), (H), and (I)] Data represent mean ± SEM, *n* = 3 independent biological replicates.

binding site on HormR/GAIN, consistent with the previous EM and molecular dynamic data. Considering that this ADGRG6+ss isoform has significantly higher basal activity (*25*) and that the rest of the receptor sequence is identical between the two isoforms, these findings provide further evidence supporting the correlation of the open ECR state with increased receptor signaling.

Recently, we reported a cancer-associated ADGRG6 mutation in the CUB domain (C94Y) near the calcium binding site (*26*). Our molecular dynamic simulations showed that the C94Y mutation destabilizes the CUB-HormR-GAIN interface, and favoring a more open conformation and signaling assays showed that this mutation increases cAMP signaling (*26*). This work is consistent with our results that the open conformation of ADGRG6 exhibits increased signaling. To test this using full-length receptors in physiological solution, we performed smFRET experiments on the C94Y receptor (−ss isoform) using the CUB and GAIN domain sensor and in the presence of 5 mM Ca^{2+}. We observed a large shift in the FRET histogram to low FRET, suggesting that the mutated receptor predominantly adopted a more open conformation (Fig. 3F). Together, these results further support the notion that the open conformation of the ECR of ADGRG6, where the CUB domain is displaced from HormR/GAIN, correlates with higher receptor activity.

Next, to specifically investigate the functional consequence of the closed ECR conformation, we engineered a disulfide bond in ADGRG6 by introducing mutations S136C and I586C to lock the receptor in a closed conformation (Fig. 3G). These residues, located in the CUB and GAIN domains, respectively, are predicted to be in close proximity based on the structure (*25*), and AlphaFold2 modeling (*44*) supported the feasibility of disulfide linkage (Fig. 3G). Consistent with the formation of a disulfide bond, smFRET analysis revealed that FRET distribution for the S136C/I586C mutant was shifted toward a higher FRET state compared to the WT receptor,

Downloaded from https://www.science.org on October 07, 2026

suggesting stabilization of the closed conformation (Fig. 3H and fig. S6, A and B). Unlike in the WT receptor, this closed conformation was retained even in 2 mM EDTA condition, confirming the stable crosslinking (fig. S6C). Functionally, this disulfide-stabilized mutant exhibited lower basal activity in cAMP assays compared to WT (Fig. 3I). This result further supports the interpretation that the closed ECR conformation correlates with a lower signaling outcome. Together, these results highlight the functional relevance of ECR conformational dynamics and demonstrate potential allosteric coupling between the ECR and the 7TM domain in ADGRG6.

Agonists stabilize the open conformation of ADGRG6

Next, we examined whether known ADGRG6 agonists influence ECR conformational dynamics within the same framework that we found for calcium. We focused on the flexible tail of prion protein C peptide (FT-PrP; sequence: KKRPKPGGWNTG) and collagen IV (Coll IV), reported to act as agonists of ADGRG6 and increase cAMP levels in cells (*37*, *39*). Specifically, previous work has shown that binding of the PrP^C to ADGRG6 in Schwann cells activates the receptor through an unknown mechanism, and this process is critical for myelination of these cells (*39*).

smFRET experiments with the CUB and GAIN domain sensor were done in the presence of 1 mM Ca^{2+} (similar to the concentration of free Ca^{2+} in the extracellular media), and increasing concentration of the FT-PrP showed a dose-dependent shift in FRET histograms toward lower values (Fig. 4A and fig. S7, A and B). Specifically, the occupancy of the low FRET state (~0.28) increased in a dose-dependent manner up to 22% in the presence of 2 mM FT-PrP (Fig. 4B). Addition of a mutated scrambled peptide (sc-PrP; sequence: AAAGAAGGWNTG), which lacks critical positively charged residues and was previously shown to be unable to activate ADGRG6 (*39*), did not alter the smFRET histogram distribution (Fig. 4, C and D, and fig. S7C). Last, similar to the prion peptide, addition of Coll IV at 100 μg/ml also shifted the FRET distribution to lower FRET values (Fig. 4, E and F, and fig. S7D). In the crystal structure, the closed conformation of ADGRG6 is stabilized via interactions from CUB, GAIN, and HormR domains, all directly or indirectly involved in coordinating and binding the calcium. Specifically, the K536 in the HormR domain interacts with E89 and D134 in the CUB domain to stabilize the calcium-binding pocket and the closed conformation (Fig. 4G). To further investigate the mechanism by which FT-PrP activates ADGRG6, we performed vbFRET analysis. We found that addition of this peptide, and not the sc-PrP, increases transitions to the low FRET state (fig. S7E). Moreover, the number of stable traces during the recording window increased only in the presence of FT-PrP, with increase only for the low FRET state (fig. S7F). Last, we performed dwell time analysis to quantify how the lifetime of different FRET states changes in the presence of FT-PrP or the sc-PrP (fig. S8). We found that the dwell time distributions fit only with a double-exponential function (fig. S8A). The long time constant (t_2) of the low and medium FRET states increased only in the presence of FT-PrP and not the scrambled PrP, while the short time constant (t_1) shows minimal changes (fig. S8B). To explore how FT-PrP or Coll IV peptide (GPRGKPGVDGYN) interacts with ADGRG6, we used AlphaFold3 modeling of the CUB domain with agonist peptides and calcium. The predicted structures showed both ligands consistently docked on the CUB domain in a configuration that would disrupt GAIN and HormR domain binding (Fig. 4, H and I). Specifically, lysine at position 5 of both peptides substitutes the role of K536 from HormR domain in coordinating key residues within the calcium binding pocket (Fig. 4, H and I). Together, these results are consistent with an activation model where agonists binding at the CUB physically inhibit closure of the ECR, thereby increasing the occupancy of the more active open conformation.

To directly test this model, we generated a receptor with an added hemagglutinin (HA)–tag after the signal peptide (at the tip of the CUB domain) (Fig. 5A). In smFRET experiments, the receptor retained similar conformational profile and dynamics as the WT receptor under Ca^{2+} or EDTA conditions (fig. S9, A to C). Addition of anti–HA-tag antibody resulted in an increase in the occupancy of the low FRET state, with further increase upon adding a secondary antibody (Fig. 5, B and C, and fig. S9, D and E). Signaling assays measuring cAMP levels and using a construct with an anti-FLAG tag after the signal peptide showed that addition of anti-FLAG antibody increased receptor signaling, with further increase after addition of a secondary antibody (Fig. 5D). Together, these results are consistent with the notion that simply impeding closure of the ECR by physical hindrance stabilizes the open conformation and increases ADGRG6 signaling.

Last, to explore how conformational dynamics at the ECR transfer to the 7TM domain, we performed smFRET experiment with a sensor labeled on the GAIN and transmembrane helix 1 (Fig. 5E). In this sensor, addition of 2 mM FT- and not the sc-PrP resulted in a statistically significant shift in the peak of the FRET histogram to higher FRET, suggesting that the conformational changes at the ECR transfer downstream to the GAIN and transmembrane domains to allosterically alter receptor signaling (Fig. 5, F and G, and fig. S10, A to D). This observation is also consistent with previous structural and dynamic studies on the holo-receptor ADGRL3 (*24*). Addition of 17-hydroxyprogesterone (17-HOP), an ADGRG6 7TMD-binding ligand previously shown to trigger Gi signaling and induce conformational changes between the extracellular loops and the extracellular domain (ECD) (*45*), produced a shift in the smFRET distribution consistent with the published mechanism (fig. S10, E to G), demonstrating that 7TMD ligand-binding competence is retained in our experimental conditions.

DISCUSSION

Allosteric communication between ligand-binding domains and active sites is a fundamental mechanism governing the activation of many receptors and enzymes. This design principle, coupling extracellular domain conformation to intracellular receptor activity, is well-established for many receptors including integrins (*46*), ionotropic receptors (*47*), and receptor tyrosine kinases such as the epidermal growth factor receptor (*48*). Leveraging this principle has been therapeutically successful, with multiple Food and Drug Administration–approved antibodies developed to stabilize specific receptor conformations (*1*, *49*). Studying the conformational dynamics of a protein is therefore essential for understanding its physiological function and enabling rational drug design.

Recent work on various aGPCRs has revealed that the conformational changes within the ECR have a direct role in receptor function. Specifically, ECRs sample different conformations that range from compact/closed to extended/open-like conformations (*22*, *25*, *26*, *29*), and these conformations correlate with different levels of receptor signaling. ADGRG6 is an aGPCR with essential roles

Downloaded from https://www.science.org on October 07, 2026

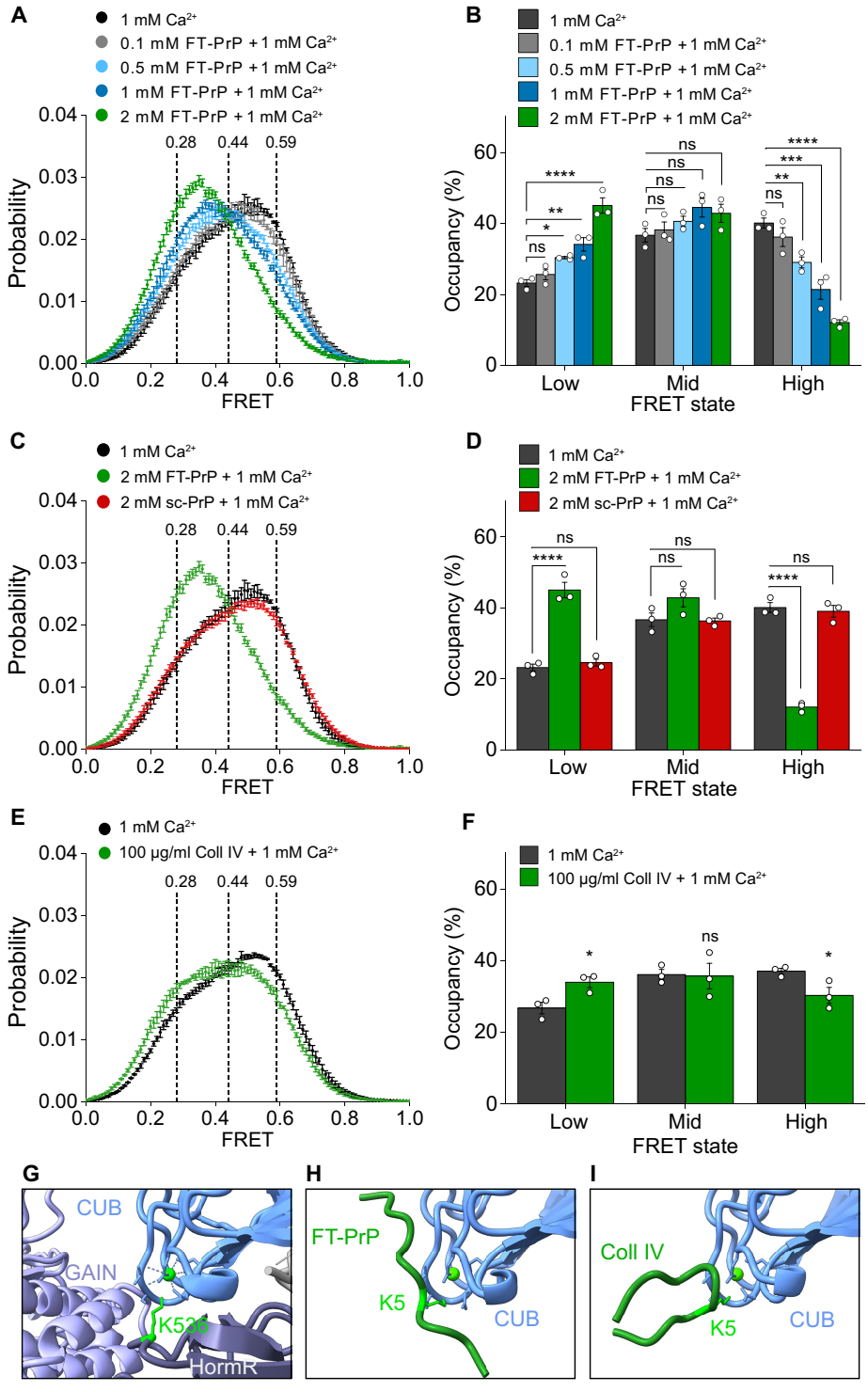

Fig. 4. Agonists stabilize the open conformation of the ECR in ADGRG6. (**A**) smFRET population histograms of data from CUB and GAIN sensor in 1 mM Ca^{2+} and FT-PrP. (**B**) Bar graph represents relative occupancy of the three conformational states. (**C**) smFRET population histograms in 1 mM Ca^{2+} and 2 mM FT-PrP or sc-PrP. (**D**) Bar graph representing relative occupancy of the three states. [(B) and (D)] Statistical significance was calculated using one-way ANOVA, Dunnett's post hoc test. $P > 0.05$ [not significant (ns)], $^{*}P < 0.05$, $^{**}P < 0.01$, $^{***}P < 0.001$, and $^{****}P < 0.0001$. (**E**) smFRET population histograms in 1 mM Ca^{2+} and Coll IV (100 µg/ml). (**F**) Quantification of occupancy of different states. Statistical significance was evaluated using a two-sample *t* test [$^{*}P < 0.05$, $P > 0.05$ (ns)]. (**G**) CUB-HormR-GAIN domain interface in ADGRG6 (PDB: 6v55) with Ca^{2+} ion and the lysine-536 on HormR domain, involved in interdomain coordination. (**H**) AlphFold3 predictions of CUB domain interaction with FT-PrP peptide (KKRPKPGGWNTG) or (**I**) with Coll IV peptide (GPRGKPGVDGYN) mediated by lysine residue 5 of these peptides. [(A) to (F)] Data represent mean ± SEM, $n = 3$ independent biological replicates.

Downloaded from https://www.science.org on October 07, 2026

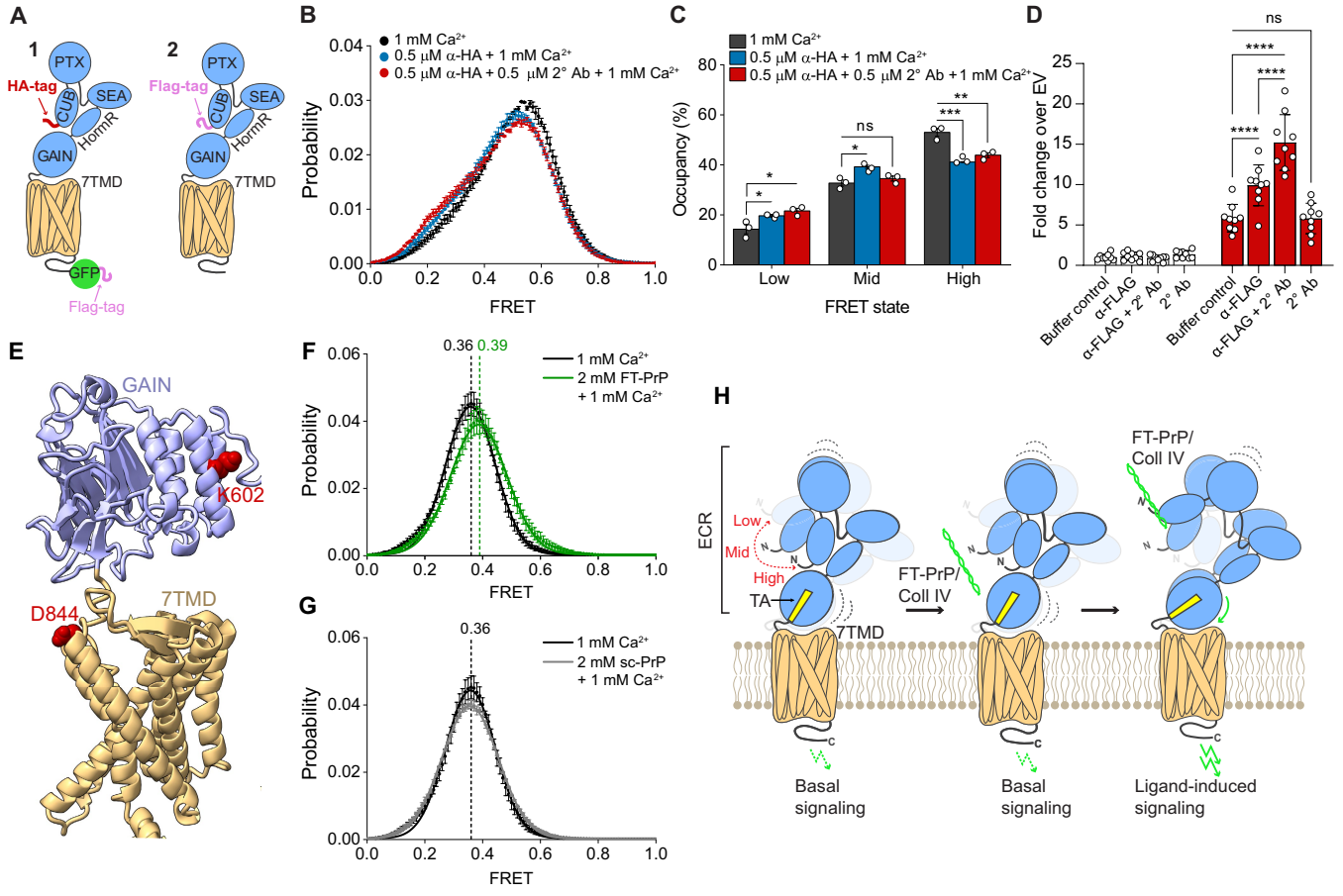

Fig. 5. Stabilizing the open conformation of the ECR in ADGRG6 in a synthetic receptor increases signaling. (**A**) Schematic of smFRET ADGRG6 construct with the HA-tag at the N terminus and GFP-Flag tag at the C terminus (1) and signaling construct with N-terminal Flag tag used for signaling experiments (2). (**B**) smFRET population histograms of CUB-GAIN domain sensor in 1 mM Ca^{2+}, with or without addition of 0.5 μM primary anti-HA antibody (α-HA) and 0.5 μM secondary antibody (2° Ab). (**C**) Bar graph representing relative occupancy of the three states in the presence of different antibodies. Statistical significance was calculated using one-way ANOVA, Dunnett's post hoc test. $P > 0.05$ (ns), $^{*}P < 0.05$, $^{**}P < 0.01$, and $^{***}P < 0.001$. (**D**) cAMP signaling activity of ADGRG6 in the absence (buffer control) or presence of α-FLAG antibody or the secondary antibody (±2° Ab). Data are expressed as fold change relative to EV and presented as mean ± SD from three independent experiments ($n = 9$). Statistical significance was determined by two-way ANOVA followed by Tukey's multiple comparisons test. $P > 0.9999$ (ns) and $^{****}P < 0.0001$. (**E**) Predicted structure of ADGRG6 GAIN and 7TMD with amino acid residues used for FRET sensor in red. (**F** and **G**) smFRET population histograms of data from sensor at GAIN-7TMD domain in 1 mM Ca^{2+} and 1 mM Ca^{2+} and 2 mM FT-PrP (F) or 1 mM Ca^{2+} and 2 mM sc-PrP (G). (**H**) Schematic of proposed model for the mechanism of allosteric activation in ADGRG6. [(B), (C), (F), and (G)] Data represent mean ± SEM of $n = 3$ independent biological replicates.

in myelination, Schwann cell, heart, and placental development. Previous work showed that different splice isoforms of ADGRG6 have distinct ECR conformations that correlate with low and high levels of downstream signaling (*25*). In a recent study, we additionally correlated an open-like conformation induced by a cancer-associated mutation with increased ADGRG6 signaling (*26*). In this study, we mapped the conformational dynamics of the ECR of −ss isoform of ADGRG6 and found that it dynamically transitions between three primary conformational states based on interdomain distance changes.

Under physiological conditions, the ADGRG6 ECR predominantly occupies a closed state, undergoing brief visits into an open, extended state (Fig. 5H). Experiments using crosslinking to constrain the receptor in the closed state reduced receptor activity, whereas an alternative isoform (ADGRG6+ss) that favors the open state exhibited enhanced signaling (*25*). The intermediate state could represent a variety of structural arrangements, including partial domain separation, hinging, interdomain rotation, or alternative domain packing that produces the observed FRET efficiency as also observed in molecular dynamic simulations of ADGRG6 ECR (*26*). While smFRET alone is limited in defining the molecular details of the conformational transitions we observe, the presence of a stable intermediate suggests a structured conformational pathway. Last, we note that the characterization of fully extended states is inherently limited by the distance sensitivity of FRET, and conformations expanding beyond this range may not be fully captured with our approach. Overall, these findings provide further support for the ECR-dependent activation mechanism of aGPCRs, showing that ECR conformation is highly correlated with signaling activity downstream of the 7TMD. These results are also in line with recent work on ADGRL3, which established the existence of multiple ECR conformational states directly correlated with distinct signaling outputs and suggesting that this conformational equilibrium, and thus signaling, can be allosterically modulated by mutations or antibodies

Downloaded from https://www.science.org on October 07, 2026

(*24*). It is likely that different splice variants of ADGRG6 with different levels of basal activity and sensitivity to activation by ligands are tuned for specific physiological roles at different developmental times and in different tissues. Considering the large number of isoforms for aGPCRs (*50*), this might be a general property of this family of receptors.

Our results provide a mechanistic model for how agonists activate ADGRG6−ss isoform. While in physiological conditions the closed conformation of the ADGRG6−ss isoform is highly stable, brief opening of the ECR is likely a mechanism for agonists such as the prion protein or type IV collagen to engage the multidomain interface consisting of CUB-GAIN-HormR domains to physically impede ECR closure, thereby increasing the occupancy of the more active open conformation (Fig. 5H). Our results and recent molecular dynamic simulations (*26*) suggest that some disease-associated mutations could also use a similar mechanism to alter ADGRG6 signaling. This mechanism highlights the CUB-GAIN-HormR interface as a potential allosteric site for developing therapeutic agonists that promote the active open state (*25*, *26*). Our result is also consistent with previous experiments that observed the activation of ADGRG6 in the presence of an anti-HA antibody or paramagnetic beads targeted to the N terminus of the receptor (*51*). While that result was attributed to the crosslinking effect of antibody or the pushing weight of the antibody, our results support a model where simply inhibiting closure of the ECR via steric hindrance due to bulky nature of the antibody can activate the receptor. Future investigations to understand the nature and mechanism of relationship between ECR conformational dynamics and Stachel-dependent activation must move beyond classical mutagenesis and focus on WT receptors. Cleavage-deficient and Stachel-modified mutants are prone to pleiotropic effects, in which sequence alterations can confound receptor folding, basal dynamics, and global ECR-7TMD architecture. Therefore, mutagenesis-based conclusions and particularly those involving the Stachel peptide should therefore be interpreted with appropriate caution. Mapping these signaling modes will instead require orthogonal biophysical and pharmacological tools that interrogate the WT receptor. For instance, residue-level behaviors can be monitored via hydrogen-deuterium exchange or nuclear magnetic resonance to reveal environmental shifts during activation by force, antibodies, or small molecules. Complementing these ensemble methods, high-resolution cryo-EM of full-length WT receptors in active conformations remains instrumental for visualizing the molecular details of ECR-TMD communication. Furthermore, the development of structure-guided nanobodies or Fabs offers a way to sterically block the Stachel-binding pocket or trap the GAIN domain in a closed conformation, modulating tethered agonism without altering the primary sequence. Alternatively, single-molecule fluorescence approaches can track ECR states and Stachel engagement in real time, while applying controlled mechanical force via optical or magnetic tweezers can directly correlate physiological force with downstream signaling in a fully native context.

Previous work identified a highly conserved calcium binding site within the CUB domain, coordinated by five residues E89, D97, D134, S136, and V137 that form a structural pocket (Fig. 1, B and C) (*25*). Disruption of this pocket disturbs the closed conformation and receptor signaling and induces severe developmental defects in zebrafish, underscoring the functional significance of ECR conformational dynamics (*25*). In most physiological contexts, the extracellular concentration of calcium is high and relatively stable; therefore, calcium is unlikely to play a regulatory role in ADGRG6 activation. By contrast, the high concentration of the extracellular matrix (ECM) adjacent to cell membranes and the dynamic nature of ECM present a plausible regulatory mechanism. ECM serves as a critical mediator for extracellular-to-intracellular signaling through interactions with receptors such as integrins, discoidin domain receptors, and leukocyte-associated immunoglobulin-like receptor-1, affecting cell proliferation, survival, and migration. Notably, the basal lamina, which is often directly adjacent to ADGRG6-expressing cells and is essential for Schwann cell myelination, is densely packed with type IV collagen, resulting in very high local concentrations of this ADGRG6 agonist (*52*, *53*). Given that the ECM undergoes substantial remodeling (*54*) during physiological processes like development, wound healing, and tissue injury, it is plausible that these dynamic changes in ECM density or composition serve as signals regulating the ECR conformational state and subsequent activation of ADGRG6.

MATERIALS AND METHODS

Molecular cloning of plasmids for smFRET

Zebrafish ADGRG6 was cloned in the pcDNA3.1(+) vector with a 14–amino acid linker at the C terminus, followed by mEGFP and Flag-tag. Construct was verified by sequencing service (ACGT Inc.). All constructs with an amber codon (TAG) mutation of amino acid at various positions (Q72, D298, I455, Y551, K602, and D844) were cloned using quickChange site-directed mutagenesis. The receptor variant ADGRG6+ss was obtained by insertion of 23–amino acid sequence by primer complimentary overlap extension cloning. The same strategy was used for cloning plasmid carrying N-terminal HA-tag. Variants with functional mutation C94Y and cysteine mutations S136C and I586C for cross-linking experiments were generated using QuickChange site-directed mutagenesis. All constructs were lastly verified with full-length sequencing (Plasmidsaurus Inc.). Cloning reagents, DNA restriction enzymes, DNA polymerase, and DNA ligase were purchased from New England Biolabs. NucleoSpin kits (Macherey-Nagel) were used for plasmid extraction and purification. All the plasmids used for smFRET experiments have an mEGFP and a FLAG-tag at the C terminus. All the plasmids for signaling have a FLAG-tag at the N terminus that is used for quantifying cell surface expression. For antibody activation smFRET experiments, an HA-tag was added at the N terminus to be compatible with these designs.

Transfection and protein expression for live cell and smFRET experiments

Following procedures previously described in (*24*), human embryonic kidney (HEK) 293T cells (Sigma-Aldrich) were kept at 37°C and 5% CO_2 in the growth media consisting of Dulbecco's modified Eagle's medium (DMEM; Gibco), 10% (v/v) cosmic fetal bovine serum (FBS) serum (Cytiva), penicillin-streptomycin (100 U/ml; Gibco), and 15 mM Hepes (pH 7.4, Gibco) and passaged every 2 to 3 days using 0.05% trypsin-EDTA (Gibco). For expression of proteins with unnatural amino acid, the growth media was supplemented with 0.25 mM trans-cyclooct-2-en-L-lysine (SiChem, #SC-8008). Twenty-four hours before transfection, HEK293T cells were seeded on poly-L-lysine–coated 18-mm glass coverslips (VWR) at 50 to 60% confluency. Next day, the media was changed to the growth media supplemented with 0.25 mM trans-cyclooct-2-en-L-lysine 2 hours before transfection. tRNA containing plasmid pNEU-hMbPylRS-

Downloaded from https://www.science.org on October 07, 2026

4xU6M15 (gift from I. Coin, Addgene, plasmid #105830) and ADGRG6 plasmid were cotransfected (1:1 w/w) using Lipofectamine 3000 (Thermo Fisher Scientific) (total plasmid: 2 μg/18 mm coverslip). After 12 hours, the growth media was exchanged with fresh media containing unnatural amino acid. After 48 hours from transfection, the unnatural amino acid supplemented media was replaced by fresh growth media and incubated for 30 min. Cells were then washed by extracellular buffer solution [128 mM NaCl, 2 mM KCl, 2.5 mM $CaCl_2$, 1.2 mM $MgCl_2$, 10 mM sucrose, and 10 mM Hepes (pH 7.4)]. Site-specific labeling was done by diluting fluorescent Cy3 and Cy5 tetrazine dyes (Vector Laboratories) to the final concentration of 30 μM each in the extracellular buffer and incubating for 15 min in the incubator. Subsequently, coverslips were gently washed by the extracellular buffer solution to remove any excess dye. For live-cell imaging, labeled cells were kept in the extracellular buffer solution. Images were taken with a Zeiss LSM800 confocal microscope with a Plan-Apochromat ×40 objective (Zeiss, 1.3 numerical aperture, oil immersion) and Zen Blue software.

Ligands and antibodies for smFRET experiments

Flexible tail of prion protein C (FT-PrP, sequence: KKRPKPGGWNTG) and nonbinding "scrambled" peptide (sc-PrP, sequence: AAAGAAGGWNTG) were synthetized by GenScript Biotech and solubilized in ultrapure water. Used peptide ligands were based on previously published data (*39*). Type IV collagen (C6745) solution was from Sigma-Aldrich. 17-HOP (Sigma-Aldrich) was dissolved in dimethyl sulfoxide at 10 mM stock concentration. Primary mouse monoclonal anti HA-tag antibody (12CA5) was purchased from Abcam, and secondary antibody [alpaca anti-mouse immunoglobulin G (IgG), 615-005-214] was from Jackson ImmunoResearch Laboratories Inc.

smFRET measurements

To identify suitable sensors for smFRET experiments, we generated a panel of constructs containing amber codon substitutions in the ECR (Xaa to TAG). Labeling sites were rationally selected to minimize structural perturbation, prioritizing solvent-exposed residues located in flexible loops and strictly avoiding buried positions within secondary structural elements. For each construct, we assessed (i) overall expression by quantifying total enhanced green fluorescent protein (EGFP) fluorescence and (ii) surface trafficking efficiency by Cy5 labeling of cell surface receptors 48 hours after expression, as described above. Mutants that retained at least 50% of total EGFP signal and exhibited Cy5 surface labeling were selected for generating double-mutant FRET sensors. All double-mutant candidates were subsequently validated using the same expression and trafficking criteria before FRET analysis.

Following procedures previously described (*24*) after labeling and washing, cells were incubated in DPBS (Dulbecco's phosphate buffered saline) without Ca^{2+}/Mg^{2+} for 15 min and then harvested by pipetting and centrifuged for 5 min, 5800*g*, at 4°C. The cell pellet was resuspended in 100 μl of lysis buffer [150 mM NaCl, 50 mM Hepes, protease inhibitor tablet containing EDTA (Thermo Fisher Scientific), and 0.1 (w/v) LMNG-CHS (10:1, Anatrace) (pH 7.4)] and lysed at 4°C for 1 hour, under gentle mixing. The cell lysate was then centrifuged for 20 min at 20,000*g* and at 4°C. The supernatant was collected and kept on ice until imaging. Cell lysate was diluted in the wash buffer [50 mM NaCl, 10 mM tris, and 0.005 (w/v) LMNG-CHS (10:1) (pH 7.35)] and was pipetted in the imaging chamber. The immobilized proteins were imaged in an imaging buffer [128 mM NaCl, 2 mM KCl, 40 mM Hepes, 4 mM Trolox, 0.005 (w/v) LMNG-CHS (10:1) (pH 7.35), and oxygen scavenging system consisting of 4 mM protocatechuic acid (Sigma-Aldrich) and bacterial protocatechuate 3,4-dioxygenase (1.6 U/ml)]. $CaCl_2$, EDTA, ligands, or antibodies were added to the imaging buffer just before application to the channel in an imaging chamber as needed. Immobilized proteins were incubated with ligands type IV collagen (Sigma-Aldrich), anti–HA-tag antibody (Abcam), or FT-PrP or scramble peptide sc-PrP for 15 to 20 min, or 0.1 mM 17-HOP (Sigma-Aldrich) for 5 min and subsequently imaged.

Imaging flow cells were assembled from glass coverslips (VWR), and microscope slides (Thermo Fisher Scientific) were assembled with mPEG (Laysan Bio) and biotin-PEG as previously described (*55*). The flow channels were functionalized with NeutrAvidin (Thermo Fisher Scientific) and biotinylated anti-GFP antibody (Abcam, ab6658). Data acquisition was carried out on a total internal reflection fluorescence microscope equipped with a 100× oil immersion objective (Olympus, numerical aperture 1.49) at 30-ms time resolution. As needed, Cy3 and Cy5 were excited with 532- and 638-nm lasers (Oxxius). Within the emission pathway, laser scattering was rejected using a 550-nm longpass filter (Chroma) and a quad-notch filter (Semrock, NF01-405/488/532/635), while donor and acceptor signals were spectrally separated using a dichroic beamsplitter (Semrock, FF640-FDi01). The 532-nm excitation intensity was 1 mW, measured at the back aperture of the objective. Brief direct acceptor excitation was done at the end of each recording to quantify the number of acceptor bleaching steps.

smFRET data analysis

Following procedures previously described in (*24*, *42*), particles with an acceptor signal upon donor excitation and with acceptor intensity greater than 10% above background were automatically selected, and donor and acceptor intensities were measured over all frames. From all detected particles (400 to 700 per movie), those which showed a single donor and a single acceptor bleaching step during the acquisition time showed stable total intensity ($I_D + I_A$), and anticorrelated donor and acceptor intensity behavior without blinking events was manually selected for further analysis (~20 to 30% of total molecules per movie). The FRET efficiency was calculated as $(I_A - 0.085 \times I_D)/[I_D + (I_A - 0.085 \times I_D)]$, where I_D and I_A are raw donor and acceptor intensities, respectively. Data were not corrected for the direct excitation of the acceptor by a 532-nm laser. Data were collected for at least three independent biological replicates, and the results were averaged, unless stated otherwise. Population smFRET histograms represent compiled data from all replicated and minimum 250 FRET traces per condition. To ensure that each trace contributes equally, the area under the FRET histogram of individual molecules was normalized to one. Error bars on histograms represent the SEM of data. Only traces longer than 5 s were kept for final data analysis to avoid bias from very short traces.

An HMM using vbFRET software was used to idealize FRET traces (*56*) and to denote the number of states. This was also corroborated with manual inspection of all the traces. Multipeak fitting analysis of population smFRET histograms was performed in OriginPro and used three Gaussian distributions as $y(x) = \sum_{i=1}^{n} \frac{A_i}{w_i\sqrt{\frac{\pi}{2}}} e^{-2\cdot\frac{(x-xc_i)^2}{w_i^2}}$,

Downloaded from https://www.science.org on October 07, 2026

where A is the peak area, w is the peak width, and xc is the peak center. Peak areas were constrained to $A > 0$. Peak widths were constrained to $0.0 < w < 0.17$ to 0.18. Peak centers were constrained by range (0.26 to 0.29, 0.42 to 0.45, and 0.57 to 0.60) of the mean FRET efficiency. A two-sample t test statistical analysis was performed in OriginPro. One-way analysis of variance (ANOVA), Dunnett's post hoc test was performed in GraphPad Prism 10.5.0.

The cross-correlation (CC) between donor and acceptor intensity traces was calculated using the equation: $CC(\tau) = \frac{\langle \delta I_D(t) \cdot \delta I_A(t+\tau) \rangle}{\langle I_D \rangle + \langle I_A \rangle}$ where τ represents the time lag, and angle brackets $\langle \ \ldots \ \rangle$ denote the time average. Intensity fluctuations were defined as $\delta I_D(t) = I_D(t) - \langle I_D \rangle$ and $\delta I_A(t) = I_A(t) - \langle I_A \rangle$. For qualitative comparison, the resulting cross-correlation curves were fitted to a single exponential decay function. The kurtosis analysis was done using the built-in function in OriginPro 9.85. For evaluation of number of states within individual traces and number of single-state traces in idealized FRET traces using vbFRET, intervals $0.01 <= x < 0.36$, $0.36 <= x < 0.50$ and $0.50 <= x < 0.99$ were chosen for the three states (CUB-GAIN sensor). Intervals $0.01 <= x < 0.62$, $0.62 <= x < 0.78$, and $0.78 <= x < 0.99$ were chosen for the CUB-PTX sensor.

For each condition, dwell times were extracted from individual traces and pooled. The cumulative distribution of dwell times was computed and converted to the complementary cumulative (survival) distribution by subtracting the cumulative count from its maximum, and the resulting distribution was then normalized to a maximum amplitude of 1. Survival distributions from at least three independent measurements were averaged, and a double-exponential decay of the form $y(x) = A_1 e^{-x/t1} + A_2 e^{-x/t2}$ was fit to the averaged survival distribution in OriginPro (OriginLab) to obtain the two time constants t_1 and t_2.

Structure visualization

Structure visualization was done using ChimeraX (*57*). For prediction of cysteine mutations S136C/I586C in the ECR of zfADGRG6, AlphaFold2 (*44*) was used with preset parameters, and the template mode was set to none. For models of CUB domain with calcium and short peptide derived from FT-PrP or type IV collagen, predictions were done using the AlphaFold Server (AlphaFold3) (*58*), with template mode set to none and otherwise preset parameters.

Signaling assay

Following procedures previously described in (*24*), HEK293 cells (American Type Culture Collection CRL-1573) were seeded in six-well plates with DMEM media supplemented with 10% (v/v) FBS and incubated at 37°C with 5% CO_2. After ~24 hours, when cells reached 50 to 60% confluency, they were cotransfected with 350 ng of the ADGRG6 construct and 350 ng of the 22F Glosensor reporter plasmid (E2301; Promega) using 2.8 μl of Fugene 6 transfection reagent (Promega). The next day, cells were washed with phosphate-buffered saline (PBS), detached with trypsin, and seeded at 5×10^4 cells per well in a white flat-bottom 96-well plate. After 24 hours, the complete medium was replaced with 100 μl of Opti-MEM Reduced-Serum Medium (Life Technologies) and incubated for 30 min. Subsequently, 1 μl of Glosensor substrate and 11 μl of FBS were added to each well. For antibody treatment experiments, 48 hours after transfection, cells were treated with α-FLAG antibody (2 μg/ml; Sigma-Aldrich, F3165) for 1 hour. The complete medium was then removed, and cells were incubated for 30 min with secondary donkey anti-mouse IgG antibody (20 μg/ml; Invitrogen, A21202) in Opti-MEM Reduced-Serum Medium. Following incubation, 1 μl of Glosensor substrate and 11 μl of FBS were added to each well. cAMP levels were measured after a 40-min equilibration period using a Synergy HTX BioTek plate reader at 25°C. Data were analyzed using GraphPad Prism 9.3.1 software and are presented as mean ± SD.

For signaling experiments with the smFRET constructs (labeling positions: 72/602, 298/455, 298/551, and 602/844) or ADGRG6-GFP-Flag, HEK293T cells were seeded in six-well plates containing DMEM media with 10% (v/v) FBS and incubated at 37°C with 5% CO_2. The following day, the media was replaced with growth media supplemented with 0.25 mM trans-cyclooct-2-en-L-lysine 2 hours before transfection. At 50 to 60% confluency, cells were cotransfected with 850 ng of the receptor construct or empty vector (EV), 850 ng of plasmid pNEU-hMbPylRS-4xU6M15, and 800 ng of the 22F Glosensor reporter plasmid using 5 μl of Lipofectamine 3000 reagent (Thermo Fisher Scientific). The following day, cells were detached by 20-min incubation in Ca^{2+}/Mg^{2+}-free DPBS, collected, and seeded in a white flat-bottom 96-well plate at a density of 5×10^4 cells per well in 100 μl of trans-cyclooct-2-en-L-lysine–containing growth media. After 24 hours, the medium was replaced with 100 μl of Opti-MEM Reduced-Serum Medium (Gibco) and incubated for 30 min at 37°C. Next, 1 μl of Glosensor substrate and 11 μl of FBS were added to each well and allowed to equilibrate for 60 min. Luminescence was measured using a Synergy Neo2 BioTek plate reader at 25°C. Data were not normalized to surface expression. Data were analyzed in OriginPro.

Flow cytometry

HEK293T cells were seeded in six-well plates and transfected at 70% confluency using a 1-μg ADGRG6 plasmid and 3-μl FuGENE 6 reagent (Promega). Following a 48-hour incubation period, cells were harvested and rinsed twice with PBS containing 0.1% bovine serum albumin (BSA; Sigma-Aldrich). Surface expression was quantified by labeling cells with mouse anti-FLAG primary antibody (Sigma-Aldrich, F3165) diluted 1:1000 in the PBS/BSA buffer for 30 min at room temperature. After three washes, the cells were stained with donkey anti-mouse Alexa Fluor 488 secondary antibody (Invitrogen; 1:500 dilution) for an additional 30 min at room temperature. Following three final washes, cells were resuspended in PBS/BSA buffer and analyzed on a BD Accuri C6 flow cytometer, recording a minimum of 5000 events per sample. Data analysis was performed using FlowJo v10, where single cells were gated and the median fluorescence intensity in the 488-nm channel was used for surface expression normalization.

Gel electrophoresis

HEK293T cells were seeded in four wells of a 12-well plate on glass coverslips. Cells expressing the CUB-GAIN sensor were prepared as described above for smFRET experiments, except that they were labeled only with Cy5 tetrazine dye. After cell lysis, the sample was centrifuged at 20,000*g* for 60 min at 4°C. The supernatant was collected, and 15 μl was mixed with 5 μl of 4× Laemmli buffer plus 10% 2-mercaptoethanol (Bio-Rad) and incubated for 20 min at room temperature. The sample was loaded into a precast 4 to 20% gradient gel (Bio-Rad) alongside 1 μl of Precision Plus protein ladder (Bio-Rad) and ran at 100 V for 2.5 hours at 4°C in 1× TGS buffer. The gel was washed in ultrapure water and imaged using a Sapphire biomolecular imager (Azure Biosystems) with 658-nm excitation wavelength and a Red710BP40 emission filter.

Downloaded from https://www.science.org on October 07, 2026

Supplementary Materials

This PDF file includes:

Figs. S1 to S10

REFERENCES

1. K. Ley, J. Rivera-Nieves, W. J. Sandborn, S. Shattil, Integrin-based therapeutics: Biological basis, clinical use and new drugs. *Nat. Rev. Drug Discov.* **15**, 173–183 (2016).
2. S. Li, K. R. Schmitz, P. D. Jeffrey, J. J. Wiltzius, P. Kussie, K. M. Ferguson, Structural basis for inhibition of the epidermal growth factor receptor by cetuximab. *Cancer Cell* **7**, 301–311 (2005).
3. J. Hamann, G. Aust, D. Arac, F. B. Engel, C. Formstone, R. Fredriksson, R. A. Hall, B. L. Harty, C. Kirchhoff, B. Knapp, A. Krishnan, I. Liebscher, H. H. Lin, D. C. Martinelli, K. R. Monk, M. C. Peeters, X. Piao, S. Promel, T. Schoneberg, T. W. Schwartz, K. Singer, M. Stacey, Y. A. Ushkaryov, M. Vallon, U. Wolfrum, M. W. Wright, L. Xu, T. Langenhan, H. B. Schioth, International union of basic and clinical pharmacology XCIV. Adhesion G protein-coupled receptors. *Pharmacol. Rev.* **67**, 338–367 (2015).
4. T. Langenhan, X. Piao, K. R. Monk, Adhesion G protein-coupled receptors in nervous system development and disease. *Nat. Rev. Neurosci.* **17**, 550–561 (2016).
5. S. Yona, H.-H. Lin, W. O. Siu, S. Gordon, M. Stacey, Adhesion-GPCRs: Emerging roles for novel receptors. *Trends Biochem. Sci.* **33**, 491–500 (2008).
6. D. Arac, A. A. Boucard, M. F. Bolliger, J. Nguyen, S. M. Soltis, T. C. Sudhof, A. T. Brunger, A novel evolutionarily conserved domain of cell-adhesion GPCRs mediates autoproteolysis. *EMBO J.* **31**, 1364–1378 (2012).
7. A. Wittlake, S. Promel, T. Schoneberg, The evolutionary history of vertebrate adhesion gpcrs and its implication on their classification. *Int. J. Mol. Sci.* **22**, 11803 (2021).
8. I. Liebscher, J. Schon, S. C. Petersen, L. Fischer, N. Auerbach, L. M. Demberg, A. Mogha, M. Coster, K. U. Simon, S. Rothemund, K. R. Monk, T. Schoneberg, A tethered agonist within the ectodomain activates the adhesion G protein-coupled receptors GPR126 and GPR133. *Cell Rep.* **9**, 2018–2026 (2014).
9. H. M. Stoveken, A. G. Hajduczok, L. Xu, G. G. Tall, Adhesion G protein-coupled receptors are activated by exposure of a cryptic tethered agonist. *Proc. Natl. Acad. Sci. U.S.A.* **112**, 6194–6199 (2015).
10. X. Barros-Alvarez, R. M. Nwokonko, A. Vizurraga, D. Matzov, F. He, M. M. Papasergi-Scott, M. J. Robertson, O. Panova, E. H. Yardeni, A. B. Seven, F. E. Kwarcinski, H. Su, M. C. Peroto, J. G. Meyerowitz, M. Shalev-Benami, G. G. Tall, G. Skiniotis, The tethered peptide activation mechanism of adhesion GPCRs. *Nature* **604**, 757–762 (2022).
11. Y. Q. Ping, P. Xiao, F. Yang, R. J. Zhao, S. C. Guo, X. Yan, X. Wu, C. Zhang, Y. Lu, F. Zhao, F. Zhou, Y. T. Xi, W. Yin, F. Z. Liu, D. F. He, D. L. Zhang, Z. L. Zhu, Y. Jiang, L. Du, S. Q. Feng, T. Schoneberg, I. Liebscher, H. E. Xu, J. P. Sun, Structural basis for the tethered peptide activation of adhesion GPCRs. *Nature* **604**, 763–770 (2022).
12. P. Xiao, S. Guo, X. Wen, Q. T. He, H. Lin, S. M. Huang, L. Gou, C. Zhang, Z. Yang, Y. N. Zhong, C. C. Yang, Y. Li, Z. Gong, X. N. Tao, Z. S. Yang, Y. Lu, S. L. Li, J. Y. He, C. Wang, L. Zhang, L. Kong, J. P. Sun, X. Yu, Tethered peptide activation mechanism of the adhesion GPCRs ADGRG2 and ADGRG4. *Nature* **604**, 771–778 (2022).
13. X. Qu, N. Qiu, M. Wang, B. Zhang, J. Du, Z. Zhong, W. Xu, X. Chu, L. Ma, C. Yi, S. Han, W. Shui, Q. Zhao, B. Wu, Structural basis of tethered agonism of the adhesion GPCRs ADGRD1 and ADGRF1. *Nature* **604**, 779–785 (2022).
14. S. Promel, M. Frickenhaus, S. Hughes, L. Mestek, D. Staunton, A. Woollard, I. Vakonakis, T. Schoneberg, R. Schnabel, A. P. Russ, T. Langenhan, The GPS motif is a molecular switch for bimodal activities of adhesion class G protein-coupled receptors. *Cell Rep.* **2**, 321–331 (2012).
15. N. Scholz, C. Guan, M. Nieberler, A. Grotemeyer, I. Maiellaro, S. Gao, S. Beck, M. Pawlak, M. Sauer, E. Asan, S. Rothemund, J. Winkler, S. Promel, G. Nagel, T. Langenhan, R. J. Kittel, Mechano-dependent signaling by Latrophilin/CIRL quenches cAMP in proprioceptive neurons. *eLife* **6**, e28360 (2017).
16. R. Sando, X. Jiang, T. C. Sudhof, Latrophilin GPCRs direct synapse specificity by coincident binding of FLRTs and teneurins. *Science* **363**, eaav7969 (2019).
17. G. Beliu, S. Altrichter, R. Guixa-Gonzalez, M. Hemberger, I. Brauer, A. K. Dahse, N. Scholz, R. Wieduwild, A. Kuhlemann, H. Batebi, F. Seufert, G. Perez-Hernandez, P. W. Hildebrand, M. Sauer, T. Langenhan, Tethered agonist exposure in intact adhesion/class B2 GPCRs through intrinsic structural flexibility of the GAIN domain. *Mol. Cell* **81**, 905–921.e5 (2021).
18. A. Kishore, R. A. Hall, Disease-associated extracellular loop mutations in the adhesion G protein-coupled receptor G1 (ADGRG1; GPR56) differentially regulate downstream signaling. *J. Biol. Chem.* **292**, 9711–9720 (2017).
19. A. Kishore, R. H. Purcell, Z. Nassiri-Toosi, R. A. Hall, Stalk-dependent and Stalk-independent signaling by the adhesion G protein-coupled receptors GPR56 (ADGRG1) and BAI1 (ADGRB1). *J. Biol. Chem.* **291**, 3385–3394 (2016).
20. K. J. Paavola, J. R. Stephenson, S. L. Ritter, S. P. Alter, R. A. Hall, The N terminus of the adhesion G protein-coupled receptor GPR56 controls receptor signaling activity. *J. Biol. Chem.* **286**, 28914–28921 (2011).
21. S. C. Petersen, R. Luo, I. Liebscher, S. Giera, S. J. Jeong, A. Mogha, M. Ghidinelli, M. L. Feltri, T. Schoneberg, X. Piao, K. R. Monk, The adhesion GPCR GPR126 has distinct, domain-dependent functions in Schwann cell development mediated by interaction with laminin-211. *Neuron* **85**, 755–769 (2015).
22. G. S. Salzman, S. D. Ackerman, C. Ding, A. Koide, K. Leon, R. Luo, H. M. Stoveken, C. G. Fernandez, G. G. Tall, X. Piao, K. R. Monk, S. Koide, D. Arac, Structural basis for regulation of GPR56/ADGRG1 by its alternatively spliced extracellular domains. *Neuron* **91**, 1292–1304 (2016).
23. G. S. Salzman, S. Zhang, A. Gupta, A. Koide, S. Koide, D. Arac, Stachel-independent modulation of GPR56/ADGRG1 signaling by synthetic ligands directed to its extracellular region. *Proc. Natl. Acad. Sci. U.S.A.* **114**, 10095–10100 (2017).
24. S. P. Kordon, K. Cechova, S. J. Bandekar, K. Leon, P. Dutka, G. Siffer, A. A. Kossiakoff, R. Vafabakhsh, D. Arac, Conformational coupling between extracellular and transmembrane domains modulates holo-adhesion GPCR function. *Nat. Commun.* **15**, 10545 (2024).
25. K. Leon, R. L. Cunningham, J. A. Riback, E. Feldman, J. Li, T. R. Sosnick, M. Zhao, K. R. Monk, D. Arac, Structural basis for adhesion G protein-coupled receptor Gpr126 function. *Nat. Commun.* **11**, 194 (2020).
26. S. J. Bandekar, E. E. Dintzner, K. Leon, S. P. Kordon, T. Slezak, K. Cechova, R. Vafabakhsh, D. Arac, The far extracellular CUB domain of the adhesion GPCR ADGRG6/GPR126 is a key regulator of receptor signaling. *Proc. Natl. Acad. Sci. U.S.A.* **122**, e2409184122 (2025).
27. Y. Zheng, D. Jiang, Y. Lu, C. Zhang, S. M. Huang, H. C. Lin, D. L. Zhang, S. C. Guo, J. F. Han, J. Chen, Y. X. He, M. X. Zhang, Y. H. Gao, Y. Y. Guo, R. Wei, M. Xia, Y. Y. Qin, Z. Q. Liu, F. Yang, S. H. Ge, F. Yi, X. Yu, H. Lin, P. Xiao, J. P. Sun, S. Q. Feng, Development of an allosteric adhesion GPCR nanobody with therapeutic potential. *Nat. Chem. Biol.* **21**, 1519–1530 (2025).
28. T. Langenhan, G. R. Anderson, D. Arac, G. Aust, M. Avila-Zozaya, S. M. Bagger, P. Barth, S. Berndt, S. C. Blacklow, B. Blanco-Redondo, A. A. Boucard, J. P. Bridges, L. S. Brodmerkel, K. M. Caron, Y. K. Chung, A. N. Dates, V. de Araujo Farias, D. Del Toro, J. G. Duman, F. B. Engel, D. M. Favara, C. J. Formstone, C. Fu, A. Garcia De Las Bayonas, A. Georgiadi, D. E. Gloriam, R. A. Hall, J. Hamann, P. W. Hildebrand, C. C. Hsiao, B. X. Huang, J. A. Javitch, H. Y. Kim, R. J. Kittel, G. Kleinau, R. Leduc, I. Liebscher, H. H. Lin, J. Linnert, M. G. Ludwig, D. C. Martinelli, S. Mathiasen, D. Matus, M. Melkumyan, A. L. Moreno-Salinas, J. Mulder, M. A. Nash, K. Pal, D. T. Pederick, N. A. Perry-Hauser, X. Piao, Y. Q. Ping, D. G. Placantonakis, F. Pohl, S. Promel, M. M. Rosenkilde, L. Sabbagh, R. C. Sando, P. Scheerer, T. Schoneberg, E. Seiradake, M. Selcho, F. Seufert, A. K. Singh, G. Skiniotis, K. Spiess, N. Strater, D. Strutt, T. C. Sudhof, J. Sun, G. G. Tall, D. Thor, D. G. Tilley, K. F. Tolias, M. Vallon, E. G. Van Meir, B. Vanhollebeke, G. R. Wiggin, U. Wolfrum, J. Yan, N. A. Zaidman, Y. Zou, N. Scholz, Adhesion G protein-coupled receptors. *Pharmacol. Rev* **78**, 100116 (2026).
29. S. J. Bandekar, K. Garbett, S. P. Kordon, E. E. Dintzner, J. Li, T. Shearer, R. C. Sando, D. Arac, Structural basis for regulation of CELSR1 by a compact module in its extracellular region. *Nat. Commun.* **16**, 3972 (2025).
30. F. S. Geng, L. Abbas, S. Baxendale, C. J. Holdsworth, A. G. Swanson, K. Slanchev, M. Hammerschmidt, J. Topczewski, T. T. Whitfield, Semicircular canal morphogenesis in the zebrafish inner ear requires the function of gpr126 (lauscher), an adhesion class G protein-coupled receptor gene. *Development* **140**, 4362–4374 (2013).
31. K. R. Monk, S. G. Naylor, T. D. Glenn, S. Mercurio, J. R. Perlin, C. Dominguez, C. B. Moens, W. S. Talbot, A G protein-coupled receptor is essential for Schwann cells to initiate myelination. *Science* **325**, 1402–1405 (2009).
32. H. Waller-Evans, S. Promel, T. Langenhan, J. Dixon, D. Zahn, W. H. Colledge, J. Doran, M. B. Carlton, B. Davies, S. A. Aparicio, J. Grosse, A. P. Russ, The orphan adhesion-GPCR GPR126 is required for embryonic development in the mouse. *PLOS ONE* **5**, e14047 (2010).
33. C. Patra, M. J. van Amerongen, S. Ghosh, F. Ricciardi, A. Sajjad, T. Novoyatleva, A. Mogha, K. R. Monk, C. Muhlfeld, F. B. Engel, Organ-specific function of adhesion G protein-coupled receptor GPR126 is domain-dependent. *Proc. Natl. Acad. Sci. U.S.A.* **110**, 16898–16903 (2013).
34. A. Mogha, A. E. Benesh, C. Patra, F. B. Engel, T. Schoneberg, I. Liebscher, K. R. Monk, Gpr126 functions in Schwann cells to control differentiation and myelination via G-protein activation. *J. Neurosci.* **33**, 17976–17985 (2013).
35. I. Kou, Y. Takahashi, T. A. Johnson, A. Takahashi, L. Guo, J. Dai, X. Qiu, S. Sharma, A. Takimoto, Y. Ogura, H. Jiang, H. Yan, K. Kono, N. Kawakami, K. Uno, M. Ito, S. Minami, H. Yanagida, H. Taneichi, N. Hosono, T. Tsuji, T. Suzuki, H. Sudo, T. Kotani, I. Yonezawa, D. Londono, D. Gordon, J. A. Herring, K. Watanabe, K. Chiba, N. Kamatani, Q. Jiang, Y. Hiraki, M. Kubo, Y. Toyama, T. Tsunoda, C. A. Wise, Y. Qiu, C. Shukunami, M. Matsumoto, S. Ikegawa, Genetic variants in GPR126 are associated with adolescent idiopathic scoliosis. *Nat. Genet.* **45**, 676–679 (2013).
36. F. Chen, J. Zhao, R. Mo, X. Ding, Y. Zhang, L. Huang, T. Xie, Y. Ding, Genetic variants in the adhesive G protein-coupled receptor ADGRG6 are associated with increased susceptibility to COPD in the elderly Han Chinese population of Southern China. *Int. J. Chron. Obstruct. Pulmon. Dis.* **19**, 2599–2610 (2024).
37. K. J. Paavola, H. Sidik, J. B. Zuchero, M. Eckart, W. S. Talbot, Type IV collagen is an activating ligand for the adhesion G protein-coupled receptor GPR126. *Sci. Signal.* **7**, ra76 (2014).

Downloaded from https://www.science.org on October 07, 2026

38. C. Wilde, P. M. Chaudhry, R. Luo, K. U. Simon, X. Piao, I. Liebscher, Collagen VI is a Gi-biased ligand of the adhesion GPCR GPR126/ADGRG6. *Cells* **12**, 1551 (2023).
39. A. Kuffer, A. K. Lakkaraju, A. Mogha, S. C. Petersen, K. Airich, C. Doucerain, R. Marpakwar, P. Bakirci, A. Senatore, A. Monnard, C. Schiavi, M. Nuvolone, B. Grosshans, S. Hornemann, F. Bassilana, K. R. Monk, A. Aguzzi, The prion protein is an agonistic ligand of the G protein-coupled receptor Adgrg6. *Nature* **536**, 464–468 (2016).
40. T. Ha, J. Y. Fei, S. Schmid, N. K. Lee, R. J. Gonzalez, S. Paul, S. Yeou, Fluorescence resonance energy transfer at the single-molecule level. *Nat. Rev. Method Primers* **4**, 21 (2024).
41. T. Moriguchi, K. Haraguchi, N. Ueda, M. Okada, T. Furuya, T. Akiyama, DREG, a developmentally regulated G protein-coupled receptor containing two conserved proteolytic cleavage sites. *Genes Cells* **9**, 549–560 (2004).
42. M. R. Schamber, R. Vafabakhsh, Mechanism of sensitivity modulation in the calcium-sensing receptor via electrostatic tuning. *Nat. Commun.* **13**, 2194 (2022).
43. B. W. Liauw, H. S. Afsari, R. Vafabakhsh, Conformational rearrangement during activation of a metabotropic glutamate receptor. *Nat. Chem. Biol.* **17**, 291–297 (2021).
44. J. Jumper, R. Evans, A. Pritzel, T. Green, M. Figurnov, O. Ronneberger, K. Tunyasuvunakool, R. Bates, A. Zidek, A. Potapenko, A. Bridgland, C. Meyer, S. A. A. Kohl, A. J. Ballard, A. Cowie, B. Romera-Paredes, S. Nikolov, R. Jain, J. Adler, T. Back, S. Petersen, D. Reiman, E. Clancy, M. Zielinski, M. Steinegger, M. Pacholska, T. Berghammer, S. Bodenstein, D. Silver, O. Vinyals, A. W. Senior, K. Kavukcuoglu, P. Kohli, D. Hassabis, Highly accurate protein structure prediction with AlphaFold. *Nature* **596**, 583–589 (2021).
45. W. An, H. Lin, L. Ma, C. Zhang, Y. Zheng, Q. Cheng, C. Ma, X. Wu, Z. Zhang, Y. Zhong, M. Wang, D. He, Z. Yang, L. Du, S. Feng, C. Wang, F. Yang, P. Xiao, P. Zhang, X. Yu, J. P. Sun, Progesterone activates GPR126 to promote breast cancer development via the Gi pathway. *Proc. Natl. Acad. Sci. U.S.A.* **119**, e2117004119 (2022).
46. P. Hu, B. H. Luo, Integrin bi-directional signaling across the plasma membrane. *J. Cell. Physiol.* **228**, 306–312 (2013).
47. D. Colquhoun, R. Lape, Perspectives on: Conformational coupling in ion channels: Allosteric coupling in ligand-gated ion channels. *J. Gen. Physiol.* **140**, 599–612 (2012).
48. E. Kovacs, J. A. Zorn, Y. Huang, T. Barros, J. Kuriyan, A structural perspective on the regulation of the epidermal growth factor receptor. *Annu. Rev. Biochem.* **84**, 739–764 (2015).
49. M. Shimaoka, T. A. Springer, Therapeutic antagonists and conformational regulation of integrin function. *Nat. Rev. Drug Discov.* **2**, 703–716 (2003).
50. C. K. Kuhn, U. Stenzel, S. Berndt, I. Liebscher, T. Schoneberg, S. Horn, The repertoire and structure of adhesion GPCR transcript variants assembled from publicly available deep-sequenced human samples. *Nucleic Acids Res.* **52**, 3823–3836 (2024).
51. J. Mitgau, J. Franke, C. Schinner, G. Stephan, S. Berndt, D. G. Placantonakis, H. Kalwa, V. Spindler, C. Wilde, I. Liebscher, The N terminus of adhesion G protein-coupled receptor GPR126/ADGRG6 as allosteric force integrator. *Front. Cell Dev. Biol.* **10**, 873278 (2022).
52. K. M. Mak, R. Mei, Basement membrane type IV collagen and laminin: An overview of their biology and value as fibrosis biomarkers of liver disease. *Anat. Rec.* **300**, 1371–1390 (2017).
53. V. S. LeBleu, B. Macdonald, R. Kalluri, Structure and function of basement membranes. *Exp. Biol. Med.* **232**, 1121–1129 (2007).
54. P. Lu, K. Takai, V. M. Weaver, Z. Werb, Extracellular matrix degradation and remodeling in development and disease. *Cold Spring Harb. Perspect. Biol.* **3**, a005058 (2011).
55. B. W. Liauw, A. Foroutan, M. R. Schamber, W. Lu, H. Samareh Afsari, R. Vafabakhsh, Conformational fingerprinting of allosteric modulators in metabotropic glutamate receptor 2. *eLife* **11**, e78982 (2022).
56. J. E. Bronson, J. Fei, J. M. Hofman, R. L. Gonzalez Jr., C. H. Wiggins, Learning rates and states from biophysical time series: A Bayesian approach to model selection and single-molecule FRET data. *Biophys. J.* **97**, 3196–3205 (2009).
57. E. C. Meng, T. D. Goddard, E. F. Pettersen, G. S. Couch, Z. J. Pearson, J. H. Morris, T. E. Ferrin, UCSF ChimeraX: Tools for structure building and analysis. *Protein Sci.* **32**, e4792 (2023).
58. J. Abramson, J. Adler, J. Dunger, R. Evans, T. Green, A. Pritzel, O. Ronneberger, L. Willmore, A. J. Ballard, J. Bambrick, S. W. Bodenstein, D. A. Evans, C. C. Hung, M. O'Neill, D. Reiman, K. Tunyasuvunakool, Z. Wu, A. Zemgulyte, E. Arvaniti, C. Beattie, O. Bertolli, A. Bridgland, A. Cherepanov, M. Congreve, A. I. Cowen-Rivers, A. Cowie, M. Figurnov, F. B. Fuchs, H. Gladman, R. Jain, Y. A. Khan, C. M. R. Low, K. Perlin, A. Potapenko, P. Savy, S. Singh, A. Stecula, A. Thillaisundaram, C. Tong, S. Yakneen, E. D. Zhong, M. Zielinski, A. Zidek, V. Bapst, P. Kohli, M. Jaderberg, D. Hassabis, J. M. Jumper, Accurate structure prediction of biomolecular interactions with AlphaFold 3. *Nature* **630**, 493–500 (2024).

Acknowledgments: We thank current and former members of the Vafabakhsh and Arac laboratories. This work made use of High Throughput Analysis Laboratory (NU-HTA) and the Keck Biophysics Facility at Northwestern University. **Funding:** This work was supported by grants R35 GM148412 (to D.A.), R01 GM140272 (to R.V.), F32 GM142266 and K99 GM157487 (to S.J.B.), and C-093 from the Chicago Biomedical Consortium (to D.A. and R.V.). G.S. is supported by the Molecular Biophysics Training Program from NIGMS/NIH (T32GM140995). **Author contributions:** Conceptualization: R.V., K.C., D.A., K.L., and M.R.S. Methodology: K.C., S.P.K., D.A., and M.R.S. Formal analysis: K.C., S.P.K., D.A., and M.F. Investigation: K.C., S.J.B., S.P.K., M.L., and M.F. Data curation: S.P.K. Validation: K.C. and D.A. Writing—original draft: K.C., R.V., and D.A. Writing—review and editing: K.C., R.V., D.A., and M.F. Visualization: K.C. and S.P.K. Supervision: R.V. and D.A. Project administration: R.V. and D.A. Resources: G.S. Software: M.R.S. Funding acquisition R.V. and D.A. **Competing interests:** The authors declare that they have no competing interests. **Data, code, and materials availability:** All data and code needed to evaluate and reproduce the results in the paper are present in the paper and/or the Supplementary Materials. All scripts used were previously published and are publicly available at the GitHub repository (https://github.com/vafabakhsh-lab/smfret-analysis) and in Zenodo at (https://doi.org/10.5281/zenodo.21707613). Representative smFRET raw data are available at the Harvard Dataverse repository (https://doi.org/10.7910/DVN/2MCIP2). Plasmids and reagents made for this study can be requested from R.V. (reza.vafabakhsh@northwestern.edu).

Submitted 24 July 2025
Accepted 8 July 2026
Published 14 August 2026
10.1126/sciadv.aea8715

Downloaded from https://www.science.org on October 07, 2026

ScienceAdvances

Ligand-tuned extracellular domain dynamics are correlated with signaling states in an adhesion GPCR

Kristina Cechova, Sumit J. Bandekar, Szymon P. Kordon, Max Foroutan, Katherine Leon, Gracie Siffer, Michael R. Schamber, Maria Luiso, Demet Araç, and Reza Vafabakhsh

Sci. Adv. **12** (33), eaea8715. DOI: 10.1126/sciadv.aea8715

View the article online
https://www.science.org/doi/10.1126/sciadv.aea8715
Permissions
https://www.science.org/help/reprints-and-permissions

Downloaded from https://www.science.org on October 07, 2026

Use of this article is subject to the Terms of service

Science Advances (ISSN 2375-2548) is published by the American Association for the Advancement of Science. 1200 New York Avenue NW, Washington, DC 20005. The title *Science Advances* is a registered trademark of AAAS.

Copyright © 2026 The Authors, some rights reserved; exclusive licensee American Association for the Advancement of Science. No claim to original U.S. Government Works. Distributed under a Creative Commons Attribution NonCommercial License 4.0 (CC BY-NC).